BER evaluation of a low-crosstalk silicon integrated multi-microring network-on-chip

Fabrizio Gambini,[1,2,*] Stefano Faralli,[1] Paolo Pintus,[1,2] Nicola Andriolli,[1] and Isabella Cerutti[1]

[1]*Scuola Superiore Sant'Anna, Via G. Moruzzi 1, 56124, Pisa, Italy*
[2]*CNIT - National Laboratory of Photonic Networks, Via G. Moruzzi 1, 56124, Pisa, Italy*
[*]*fabrizio.gambini@sssup.it*

Abstract: The operation of an integrated silicon-photonics multi-microring network-on-chip (NoC) is experimentally demonstrated in terms of transmission spectra and bit error rates at 10 Gb/s. The integrated NoC consists of 8 thermally tuned microrings coupled to a central ring. The switching functionalities are tested with concurrent transmissions at both the same and different wavelengths. Experimental results validate the analytical model based on the transfer matrix method. BER measurements show performance up to 10^{-9} at 10 Gb/s with limited crosstalk and penalty (below 0.5 dB) induced by an interfering transmission.

OCIS codes: (130.0130) Integrated optics; (130.4815) Optical switching devices; (200.4650) Optical interconnects.

References and links

1. P. P. Pande, C. Grecu, M. Jones, A. Ivanov, and R. Saleh, "Performance evaluation and design trade-offs for network-on-chip interconnect architectures," IEEE Trans. Comput. **54**(8), 1025–1040 (2005).
2. A. Biberman, H. L. R. Lira, K. Padmaraju, N. Ophir, J. Chan, M. Lipson, and K. Bergman, "Broadband silicon photonic electrooptic switch for photonic interconnection networks," IEEE Photon. Technol. Lett. **23**(8), 504–506 (2011).
3. B. G. Lee, A. Biberman, J. Chan, and K. Bergman, "High-performance modulators and switches for silicon photonic networks-on-chip," IEEE J. Sel. Top. Quantum Electron. **16**(1), 6–22 (2010).
4. A. Shacham, K. Bergman, and L. P. Carloni, "Photonic networks-on-chip for future generations of chip multiprocessors," IEEE Trans. Comput. **57**(9), 1246–1260 (2008).
5. R. G. Beausoleil, J. Ahn, N. Binkert, A. Davis, D. Fattal, M. Fiorentino, N. P. Jouppi, M. McLaren, C. M. Santori, R. S. Schreiber, S. M. Spillane, D. Vantrease, and Q. Xu, "A nanophotonic interconnect for high-performance many-core computation," in Proc. IEEE Symposium on High Performance Interconnects, 182–189 (2008).
6. N. Kirman, M. Kirman, R. K. Dokania, J. F. Martinez, A. B. Apsel, M. A. Watkins, and D. H. Albonesi, "On-Chip optical technology in future bus-based multicore designs," IEEE Micro **27**(1), 56–66 (2007).
7. P. Dong, Y. Chen, T. Gu, L. Buhl, D. Neilson, and J. Sinsky, "Reconfigurable 100 Gb/s silicon photonic network-on-chip [Invited]," IEEE J. Opt. Commun. Netw. **7**(1), A37–A43 (2015).
8. A. Joshi, C. Batten, Y.-J. Kwon, S. Beamer, I. Shamim, K. Asanovic, and V. Stojanovic, "Silicon-photonic clos networks for global on-chip communication," in Proc. NoCS (2009).
9. D. Nikolova, S. Rumley, D. Calhoun, Q. Li, R. Hendry, P. Samadi, and K. Bergman, "Scaling silicon photonic switch fabrics for data center interconnection networks," Opt. Express **23**(2), 1159–1175 (2015).
10. A. Parini, G. Bellanca, A. Annoni, F. Morichetti, A. Melloni, M. J. Strain, M. Sorel, M. Gay, C. Pareige, L. Bramerie, and M. Thual, "BER evaluation of a passive SOI WDM router," IEEE Photon. Technol. Lett. **25**(23), 2285–2288 (2013).
11. N. Sherwood-Droz, H. Wang, L. Chen, B. G. Lee, A. Biberman, K. Bergman, and M. Lipson, "Optical 4x4 hitless silicon router for optical networks-on-chip (NoC)," Opt. Express **16**(20), 15915–15922 (2008).
12. H. Subbaraman, X. Xu, A. Hosseini, X. Zhang, Y. Zhang, D. Kwong, and R. T. Chen, "Recent advances in silicon-based passive and active optical interconnects," Opt. Express **23**(3), 2487–2511 (2015).
13. P. Pintus, P. Contu, P. G. Raponi, I. Cerutti, and N. Andriolli, "Silicon-based all-optical multi microring network-on-chip," Opt. Lett. **39**(4), 797–800 (2014).
14. F. Gambini, P. Pintus, S. Faralli, N. Andriolli, and I. Cerutti, "Demonstration of a photonic integrated network-on-chip with multi microring," in Proc. Optical Fiber Communications (OFC) conference (2015).
15. S. Faralli, F. Gambini, P. Pintus, I. Cerutti, and N. Andriolli, "Ring Versus Bus: A BER Comparison of Photonic Integrated Networks-on-Chip," in Proc. Optical Interconnects (2015).

#236797 Received 27 Mar 2015; revised 15 May 2015; accepted 25 May 2015; published 23 Jun 2015

16. M. R. Watts, W. A. Zortman, D. C. Trotter, G. N. Nielson, D. L. Luck, and R. W. Young, "Adiabatic resonant microrings (ARMs) with directly integrated thermal microphotonics," in Proc. CLEO/QELS (2009).
17. G. Cocorullo, F. G. Della Corte, and I. Rendina, "Temperature dependence of the thermo-optic coefficient in crystalline silicon between room temperature and 550 K at the wavelength of 1523 nm," Appl. Phys. Lett. **74**(22), 3338 (1999).
18. COMSOL, Multiphysics, www.comsol.com
19. D. T. Spencer, J. F. Bauters, M. J. R. Heck, and J. E. Bowers, "Integrated waveguide coupled Si_3N_4 resonators in the ultrahigh-Q regime," Optica **1**(3), 153–157 (2014).
20. Y. Wang, J. Flueckiger, C. Lin, and L. Chrostowski, "Universal grating coupler design," in Proc. SPIE Photonics North (2013).
21. W. Bogaerts, P. De Heyn, T. Van Vaerenbergh, K. De Vos, S. Kumar Selvaraja, T. Claes, P. Dumon, P. Bienstman, D. Van Thourhout, and R. Baets, "Silicon microring resonators," Laser Photonics Rev. **6**(1), 47–73 (2012).

1. Introduction

Over the last decade, the evolution of computing systems has been fostered by the integration of multiple processors onto a single die, enabling the steady performance increase predicted by Moore's law. In multi- and many-core architectures, not only does the overall performance of the computing system depend on the capabilities of the processing nodes, but it relies more and more on the electrical network-on-chip (NoC) carrying the communications among processors and between processors and memories. The existing electrical NoCs are already showing their limitations such as high and non-uniform communication latency, high power consumption, and large footprint [1].

To overcome the above mentioned limitations photonic integrated solutions are currently investigated. Silicon (Si) photonic integrated technology is promising for limiting the power consumption and the footprint of NoC and for supporting high transmission rates while benefiting from a low-cost, high-volume production lines with the complementary metal-oxide-semiconductor (CMOS) compatibility [2, 3].

Several photonic NoC architectures have been proposed in the literature, enabling the exchange of optical packets among processors and memories. A photonic integrated circuit (PIC)-switched network carrying large messages was presented in [4], requiring however a rather slow circuit set up process performed on a parallel electrical interconnection network. Various crossbar architectures have been proposed [5], implemented with a large number of parallel bus waveguides. An opto-electronic bus network was designed in [6] exploiting wavelength division multiplexing (WDM) to boost the capacity and bandwidth density. Also in [7] a reconfigurable photonic integrated WDM bus NoC has been proposed and experimentally demonstrated up to 100 Gb/s. However bus topologies need to be significantly overprovisioned to effectively support all-to-all communications. For this reason, multistage silicon photonics switching matrices have been proposed. Clos-based architectures have been studied, however their latency is affected by the crossing of multiple switching stages [8]. Cascaded switches based on microring structures and waveguide crossings have been evaluated in [9] and tested up to 10 Gb/s in concurrent multi-wavelength scenario in [10]. Despite their low crosstalk [11], in architectures with multiple waveguide intersections the quality of the signal can be seriously affected. Unfortunately, the crossing crosstalk can be mitigated only by increasing fabrication complexity and costs [12].

An optical NoC architecture that avoids waveguide crossing and ensures path uniformity in terms of crossed switched elements is the recently proposed multi-microring (MMR) network-on-chip [13]. This architecture is based on a ring topology, which is realized with a central microring accessed by coupling the signal with local microrings, or simply local rings. MMR exploits WDM transmissions, is suitable for concurrent transmissions on the same and different wavelengths and enables the possibility to transmit and receive simultaneously at each port. The performance computed in terms of transmission spectra using a mathematical model based on transfer matrix method estimates low crosstalk, making MMR suitable for concurrent transmissions at the same wavelength. The model indicates also that a good trade-

#236797 Received 27 Mar 2015; revised 15 May 2015; accepted 25 May 2015; published 23 Jun 2015

off between bandwidth and crosstalk can be achieved by properly selecting the coupling coefficient between central and local rings. Supported by the promising numerical results, the MMR architecture was then fabricated.

The fabricated PIC is a proof of concept of the proposed MMR architecture. This paper aims to experimentally validate such proof of concept and extends the results in [14,15] derived for transmissions on a single wavelength. More specifically, the experimental characterization of the integrated Si-based MMR NoC are reported in terms of both transmission spectra and bit error rate (BER) measured for single-wavelength and multiple-wavelength concurrent transmissions at 10 Gb/s. Cross-validation of numerical and experimental results is also carried out by comparing simulated and measured transmission spectra.

2. Device architecture and design

The considered MMR NoC consists of a central microring connecting eight thermally tuned local microrings, as shown in Fig. 1(a). In each pair of local microrings, one ring (T*i* in Fig. 1(a), for $i = 1,2,3,4$) enables the communication of the optical signal from the *i-th* transmitter to the central ring, whereas the other (R*j* in Fig. 1(a), for $j = 1,2,3,4$) connects the central ring to the receiver. All the local rings are coupled to the central ring, which acts as a shared waveguide enabling the propagation of the optical signals from any transmitter to any receiver. In this architecture, the signal transmitted by T*i* is guided from the central ring and then it is dropped at the intended R*j*. Each local ring is also coupled to a local waveguide whose terminations act as either input or output ports: one port is connected to the transmitter or to the receiver, whereas the other one (dummy port) can be used for testing (e.g., for controlling the resonance shift of the ring).

The MMR NoC is designed with identical local rings of 10 μm radius. The ratio between the free spectral range of a local ring and of the central ring is 4. Based on the analytical model in [13], a coupling coefficient of 10% is selected in order to achieve a good trade-off between bandwidth and crosstalk, while guaranteeing a design robust to fabrication inaccuracies.

The cross-section of the local rings is schematically shown in Fig. 1(b), consisting of a 480-nm-wide single-mode half-rib waveguide. Each local ring can be independently tuned by exploiting the Joule effect induced by the electrical current injection in the doped 90-nm-thick internal slab [16]. The resonance wavelength shift $\Delta\lambda$ due to the temperature variation ΔT can be estimated as

$$\frac{\Delta\lambda}{\lambda} = \frac{1}{n_g}\left(\frac{\partial n_{eff}}{\partial n_{core}}\frac{\partial n_{core}}{\partial T} + \frac{\partial n_{eff}}{\partial n_{clad}}\frac{\partial n_{clad}}{\partial T}\right)\Delta T, \tag{1}$$

where λ is the resonant wavelength, n_{eff} and n_g are the effective and the group indices of the propagation mode, respectively. The derivatives $\partial n_{eff}/\partial n_{core}$ and $\partial n_{eff}/\partial n_{clad}$ are the variations of the effective index with respect to the core and cladding refractive indices, whereas the derivatives $\partial n_{core}/\partial T$ and $\partial n_{clad}/\partial T$ relates the refractive indices of core and cladding respectively, to the temperature. The variations $\partial n_{eff}/\partial n_{core}$ and $\partial n_{eff}/\partial n_{clad}$ depend on the core-cladding refractive index contrast and on the geometry of the waveguide, whereas the variations $\partial n_{core}/\partial T$ and $\partial n_{clad}/\partial T$ depend only on the materials and take value equal to $2\cdot10^{-4}$/K and$1\cdot10^{-5}$/K for silicon and silica, respectively [17]. The cylindrical mode solver computed $n_{eff} = 2.37$, $n_g = 3.8$, $\partial n_{eff}/\partial n_{core} = 0.25$ and $\partial n_{eff}/\partial n_{clad} = 1.0$ for the TE fundamental mode at $\lambda = 1550$nm. As a result, a wavelength shift of one FSR requires a temperature variation of about 115 °C, corresponding to a thermal efficiency of 0.08 nm/°C. The integrated conductive paths (indicated in Fig. 1(b) and in Fig. 1(c)) were simulated using COMSOL® multiphysics tools [18]. The increment of temperature with the electrical current was assessed using 3D_simulations. Among the different simulated configurations, it was

#236797 Received 27 Mar 2015; revised 15 May 2015; accepted 25 May 2015; published 23 Jun 2015

selected the layout that maximizes the tuning efficiency while accounting for the technological constraints.

The cross-section of central microring is a 460-nm-wide single-mode ridge (see Fig. 1(b)). Due to the technological limitation on the minimum inter-waveguide gap width (200 nm), it has been necessary to lengthen the coupling region by bending the coupled waveguide. Using finite-difference time-domain (FDTD) simulations, an angle of 32° [19] was found to achieve the optimum coupling coefficient that enables the maximization of the transmission bandwidth with a limited crosstalk.

The PIC was fabricated at the Institute of Microelectronics (IME), Singapore, through CMC Microsystems as part of a multi-project wafer run on 220-nm SOI platform. A picture of a single microring is reported in Fig. 1(c). The footprint of the MMR network-on-chip is 105 × 105 μm^2. Two arrays of eight single-mode TE grating couplers with a coupling insertion loss of 5 dB [20] are used to couple light in and out from the chip, whereas ten Al/TaN pads are used to independently tune the eight local rings.

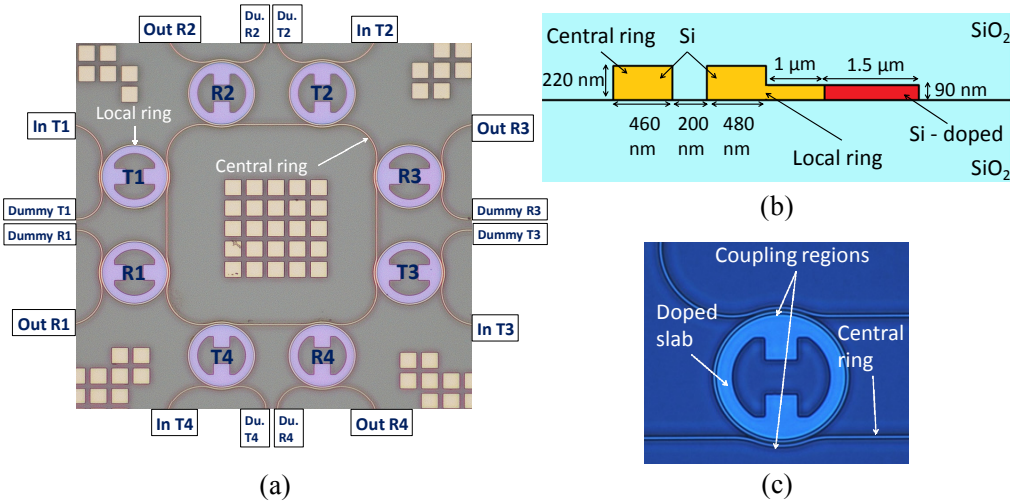

Fig. 1. Microscopy photo of the realized MMR NoC architecture (with the port names) (a), device cross section scheme (b), and microscopy photo of a local ring in which the coupling regions and the silicon doped slab are clearly visible (c). For display purposes, the devices in the pictures do not include the metal layer and the contact pads.

3. Measurements and discussions

Measurements and characterization of the MMR NoC have been carried out first on a single local ring, and then on the entire MMR NoC with concurrent transmissions at both the same and different wavelengths. For the single local ring, the testbed setup is shown in Fig. 2, aimed at performing a spectral characterization. PICs are characterized at room temperature. A continuous wave signal is generated by an external cavity tunable laser (TL) in the range between 1530 nm and 1570 nm with a power of 7 dBm and is optionally amplified by an erbium doped fiber amplifier (EDFA). The signal is then coupled into the input grating coupler of the ring using a polarization controller (PC). The output spectrum is taken with a synchronized power meter.

The spectral response measured at the different output ports of the local ring is plotted in Fig. 3(a). The 3-dB bandwidth is 37 GHz, the free-spectral-range (FSR) is about 9.62 nm and the backscattered signal is suppressed by a factor of 20 dB. The resonance wavelength shift with respect to the electrical dissipated power is reported in Fig. 3(b). Measurements are obtained by injecting current into the doped path of the ring and measuring the wavelength shift of the resonance. The measured data (red squares) are in good agreement with the results

#236797 Received 27 Mar 2015; revised 15 May 2015; accepted 25 May 2015; published 23 Jun 2015

of the simulation described in the previous section (solid blue line), with a small discrepancy mainly caused by the doping inaccuracies. The tuning efficiency is about 189 pm/mW, which means that a complete FSR shift requires about 50.8 mW of dissipated power.

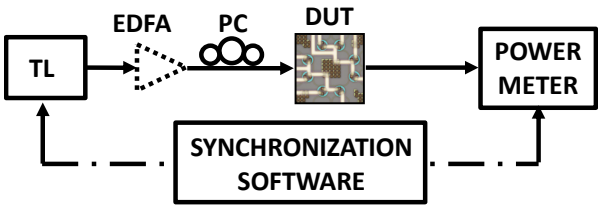

Fig. 2. Experimental setup for spectrum characterizations.

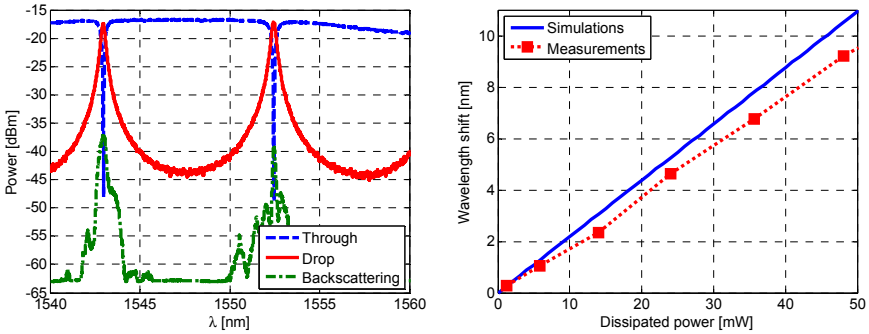

Fig. 3. Spectral response of a 10-μm radius local ring (a), and wavelength shift as a function of the electrical dissipated power for simulated (solid blue line) and measured data (red squares) (b).

To fully characterize the entire MMR NoC, two configurations are investigated: (i) single-wavelength transmissions and (ii) two-wavelength transmissions. For both configurations the worst-case scenario from the crosstalk point of view is considered [13]. In the single-wavelength configuration, two transmissions take place between adjacent ring pairs: from T1 to R2 and from T4 to R1. In the two-wavelength configuration, the transmissions occur from T1 to R3 on wavelength λ_1 and from T4 to R2 on wavelength λ_2. In these experiments, two 8-port fiber arrays are used to couple the light in/out from the PIC, enabling the access to the input, output and dummy ports. Moreover, a 10-pin DC probe array is used to independently tune the 8 local rings. Two types of measurements have been carried out on the MMR NoC. First, transmission spectra are measured through the same setup shown in Fig. 2 to compare experimental results with the ones derived with the transfer matrix approach described in [13]. Then, the system-level performance of both configurations is assessed, using the experimental setup in Fig. 4. OOK signals at 10 Gb/s are utilized, as envisioned in [5]. For the single-wavelength configuration, an external cavity tunable laser (TL) provides a continuous wave optical signal with an optical power of 10 dBm at the wavelength λ_1 = 1548.208 nm. The optical power is split in two arms by a 3-dB optical splitter and modulated by two different Mach-Zehnder interferometers (MZI). For the two-wavelength configuration, two different TLs provide two continuous wave signals with an optical power of 7 dBm at λ_1 = 1548.208nm and λ_2 = 1550.420nm. In either configuration, the TL linewidth is set to 100 MHz by activating the coherence control. The signals pass through a polarization controller (PC) before being modulated by two MZIs, which are fed by a bit-pattern-generator (BPG) at 10 Gb/s with a pseudo-random binary sequence (PRBS) long 2^{31}-1. The two bit streams are decorrelated using a 50-m single-mode fiber (SMF) on one arm only (the lower arm in the

#236797 Received 27 Mar 2015; revised 15 May 2015; accepted 25 May 2015; published 23 Jun 2015

figure). Each signal is then amplified by an EDFA and filtered by an optical bandpass filters (OBPF) with 1 nm bandwidth. Variable optical attenuators (VOA) allow for the equalization of the optical power at the two PIC inputs. The signals are then polarization controlled (PC) before being coupled to the PIC. The receiver front-end is composed by a cascade of an EDFA, a 1.2-nm and 4-nm wide OBPF (for the single-wavelength and two-wavelength configuration, respectively), a VOA and a PIN photodiode.

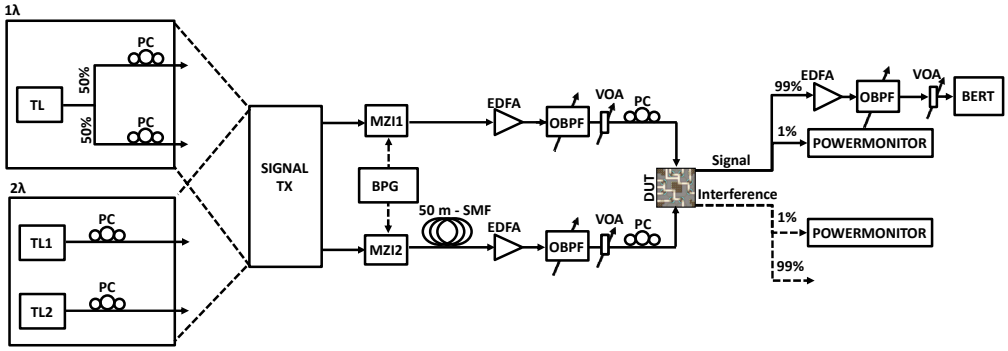

Fig. 4. Experimental setup for BER measurements in single-wavelength and two-wavelength configurations.

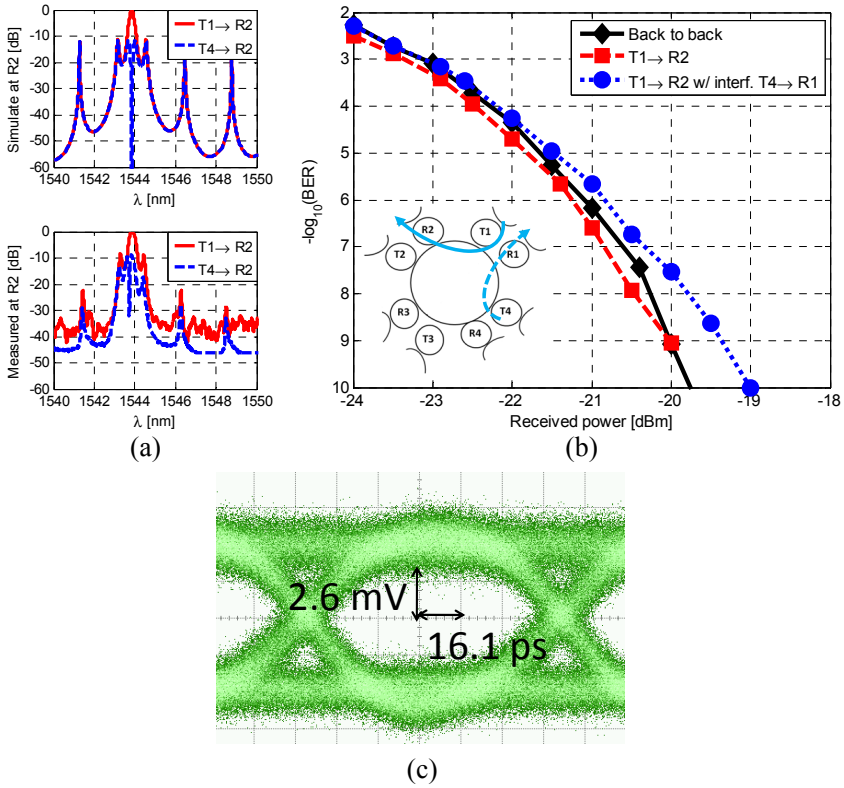

Fig. 5. MMR in single-wavelength configuration: simulated and measured transmission spectra normalized to the grating coupler insertion loss for transmissions T1→R2 (signal) and T4→R2 (interference) (a), the corresponding BER vs. received power curves at 10 Gb/s (b), and eye diagram for transmission T1→R2 with the concurrent interfering transmission T4→R1 at the same wavelength, at BER of 10^{-8} (c).

#236797 Received 27 Mar 2015; revised 15 May 2015; accepted 25 May 2015; published 23 Jun 2015

Figures 5 and 6 focus on the single-wavelength configuration, where all the local rings are tuned to the same wavelength in order to evaluate the homo-wavelength crosstalk. The effect on the expected transmission (i.e., T1→R2) of the interference caused by another transmission on the same wavelength is assessed, i.e., an adjacent upstream transmission T4→R1 in Fig. 5, and a non-adjacent upstream transmission T3→R4 in Fig. 6. Indeed the signal of the upstream transmission may not be completely dropped at the intended receiver (R1 in Fig. 5 and R4 in Fig. 6), causing interference on expected transmission T1→R2. Figures 5(a) and 6(a) show the simulated and measured transmission spectra for the expected transmission and the considered interfering transmission, and exhibit a very good agreement between theory and experiments. The measured 3-dB bandwidth related to the transmission T1→R2 is equal to 39 GHz, very close to the simulated bandwidth of 40 GHz. The most detrimental homo-wavelength crosstalk [13,14] is induced by the upstream transmission T4→R1, which generates a homo-wavelength crosstalk of −12 dB at receiver R2.

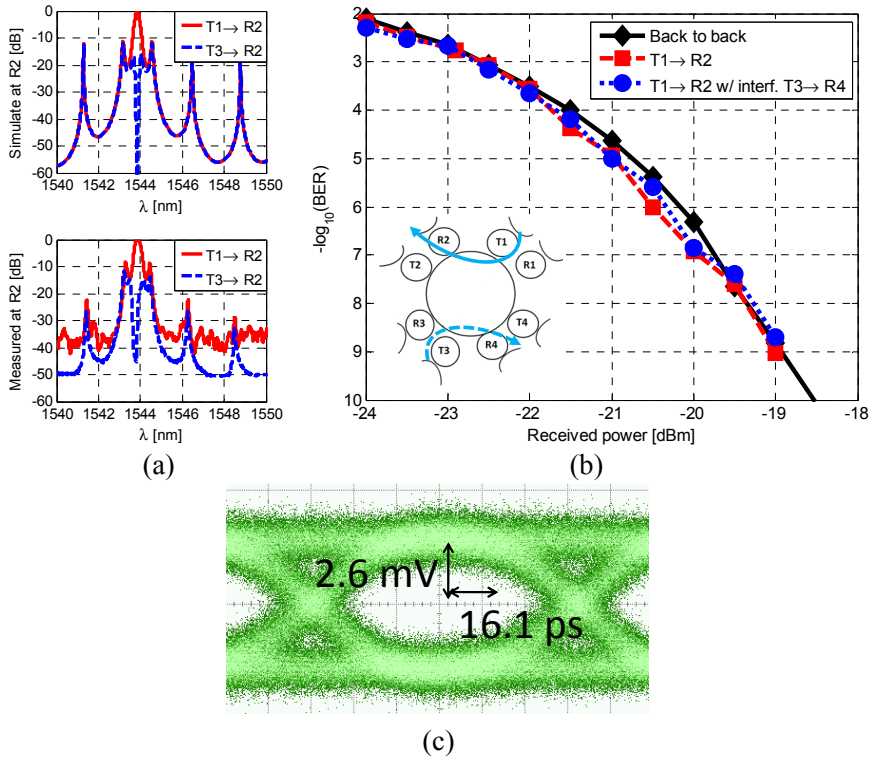

Fig. 6. MMR in single-wavelength configuration: simulated (top) and measured (bottom) transmission spectra normalized to the grating coupler insertion loss for transmissions T1→R2 (signal) and T3→R2 (interference) (a), the related BER vs. received power curves at 10 Gb/s (b), and eye diagram for 10 Gb/s for transmission T1→R2 with the concurrent interfering transmission T3→R4 at the same wavelength, at a BER of 10^{-8} (c).

Figures 5(b) and 6(b) evaluate the system performance in terms of BER for the single-wavelength configuration in the presence and absence of the interfering transmission. Measurements are performed as a function of the received power with a constant optical signal-to-noise ratio (OSNR). Back to back curve is reported as reference. The insets of the plots show the transmission paths in the MMR. For the case in Fig. 5(b), the square and circle marked curves refer to the transmission without and with interfering transmission (i.e., T4→R1), respectively. The BER in absence of interfering transmission (i.e., T1→R2 only)

#236797 Received 27 Mar 2015; revised 15 May 2015; accepted 25 May 2015; published 23 Jun 2015

outperforms the BER in back to back. This improvement is due to the filtering effect of the traversed rings, acting as an adapted receiver [10]. BER of transmission T1→R2 is affected by the concurrent upstream transmission T4→R1 at the same wavelength. The impact of the interfering transmission is visible but limited to about 0.5 dB of penalty for a BER of 10^{-9}. Eye diagram related to the transmission T1→R2 in presence of the interfering transmission T4→R1 is reported in Fig. 5(c) and shows a clear eye opening. In Fig. 6(b), the performance degradation on the transmission T1→R2 is mitigated with respect to the case in Fig. 5(b), and no BER penalty can be appreciated. The reason is due to the fact that the residual signal from T3→R4 transmission must travel a longer path before reaching destination R2. The filtering effect of the local rings along the path enables a homo-wavelength crosstalk at R2 as low as −19 dB. This crosstalk level is properly predicted by the simulation results. In Fig. 6(c) the eye diagram for the transmission T1→R2 in the presence of the interfering transmission T3→R4 is reported and shows a clear eye aperture.

Figures 7(a) and 7(b) present the spectral and BER performance, respectively, for the two-wavelength configuration. In order to evaluate the hetero-wavelength crosstalk the MMR NoC is tuned to support two concurrent transmissions on partially overlapping paths (i.e., the worst-case scenario for two-wavelength transmission): T1→R3 on λ_1 = 1548.208 nm and T4→R2 on λ_2 = 1550.420 nm, corresponding to an inter-channel gap of 301.5 GHz. Results in terms of transmission spectra are shown in Fig. 7(a), where simulations (top subfigures) are compared to measurements (bottom subfigures). A very good agreement between simulated and experimental results is attained for this configuration too. A summary of the simulated and experimental performance for the two-wavelength scenario is reported in Table 1. The measured 3-dB bandwidth for the transmissions T1→R3 at λ_1 and T4→R2 at λ_2 are 31 GHz and 22 GHz, while the measured crosstalk levels are −37 dB and −19 dB for the two transmissions, respectively. The small mismatches between theoretical and experimental results can be evaluated in Table 1 and they are mainly related to fabrication and tuning inaccuracies.

Figure 7(b) assesses the BER performance for the two concurrent and partially superimposed transmissions at two different wavelengths. Back to back BER are reported for reference. The small discrepancy of the back to back BER values at the two different wavelengths is due to the different transmission blocks (TL, MZI, EDFA, OBPF). Similarly, the difference of BER between the curves related to transmissions T1→R3 and T4→R2 is due to the different transmission blocks. As shown, the transmission T1→R3 at λ_1 does not degrade the transmission T4→R2 at λ_2. Similarly, the same behavior is observed for the transmission T1→ R3, with and without the interfering transmission T4→R2 at a different wavelength. Finally, Figs. 7(c) and 7(d) show the eye diagram for transmissions T4→R2 and T1→R3, respectively at two different wavelengths, in the presence of concurrent transmission on the other wavelength. Contrary to Fig. 5, in Figs. 6 and 7 the BER curves for the single-transmission do not outperform the B2B results. This can be explained by the technical difficulty of achieving the same OSNR in the experimental setup with the PIC. Indeed the OSNR for the single-transmission cases was about 33 dB, which is lower than the OSNR of 39 dB for the back to back case.

Table 1. Simulated and measured 3-dB bandwidth and crosstalk levels for two-wavelength configuration[a].

Configuration		Simulated 3-dB bandwidth	Measured 3-dB bandwidth	Simulated crosstalk level	Measured crosstalk level
Two wavelengths	λ1	25 GHz	31 GHz	–42 dB	–37 dB
	λ2	23 GHz	22 GHz	–23 dB	–19 dB

#236797 Received 27 Mar 2015; revised 15 May 2015; accepted 25 May 2015; published 23 Jun 2015

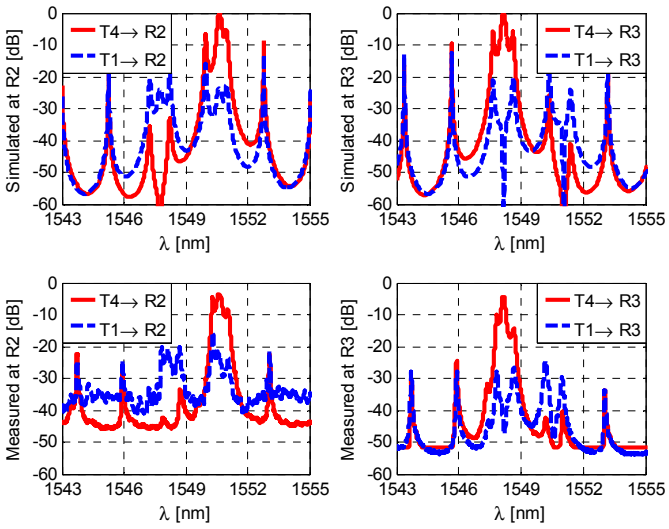

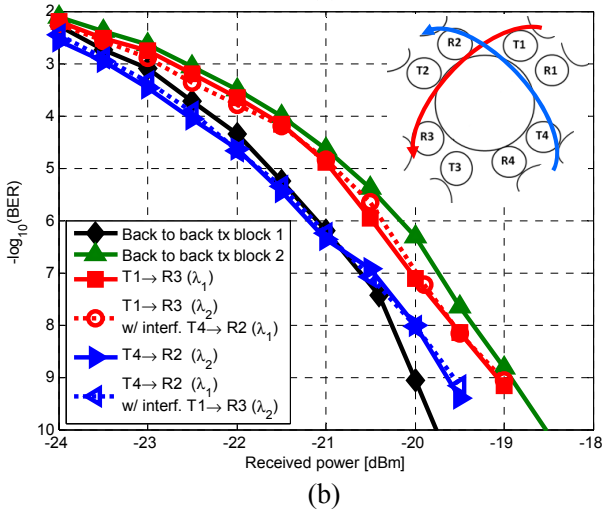

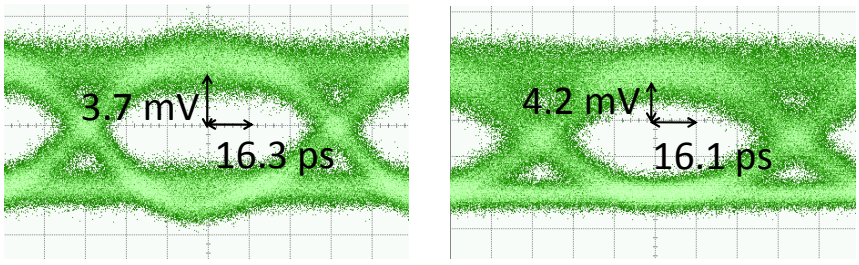

Fig. 7. MMR in two-wavelength configuration: simulated (top) and measured (bottom) transmission spectra normalized to the grating coupler insertion loss for transmissions T4→R2 and T1→R3 (signals) with the interference contributions T1→R2 and T4→R3, respectively (a), the corresponding BER vs. received power curves at 10 Gb/s (b). In (c) and (d) the eye diagrams to for transmission T4→R2 and T1→R3 (in presence of their interfering transmission), respectively, at BER of 10^{-8}.

#236797 Received 27 Mar 2015; revised 15 May 2015; accepted 25 May 2015; published 23 Jun 2015

4. Conclusions

An integrated photonic multi-microring NoC has been designed and fabricated on a SOI platform. The theoretical model based on the transfer matrix method has been validated through experimental results in terms of transmission spectra. Transmissions at 10 Gb/s have been assessed in terms of BER for both single-wavelength and multi-wavelength configurations. The experimental characterization demonstrates that not only the fabricated MMR NoC achieves the predicted performance and supports a single transmission with a good BER performance, but also that multiple concurrent transmissions can coexist on the same wavelength (provided that they path are disjoint) and on different wavelengths with a low homo and hetero-wavelength crosstalk. This work demonstrates that wavelength division multiplexing and spatial reuse of the same wavelength can be effectively exploited for the transmission, enabling a high NoC throughput. Further work will aim to reduce the technical difficulties encountered during the testing (for instance using a customized packaging for the PIC) and to assess the scalability of the NoC. Also a further design by using different microring tuning technique [21] and different technological foundry rules can improve the performance in terms of power efficiency, footprint, and packaging issues.

Acknowledgments

This work is partially supported by the Italian Ministry of Education, University and Research (MIUR) through the FIRB project “MINOS”, by the Italian Ministry of Foreign Affairs (MAE-UST) through the high-relevance bilateral project “NANO-RODIN”, and by the European Commission through the FP7 project IRIS (no. 619194). The authors acknowledge NSERC SiEPIC Program for the training and the component library, and CMC Microsystems for the foundry service and fruitful technical discussions.

#236797 Received 27 Mar 2015; revised 15 May 2015; accepted 25 May 2015; published 23 Jun 2015